Available online at www.sciencedirect.com
SCIENCE DIRECT®
Polymer 44 (2003) 4239–4247
polymer
www.elsevier.com/locate/polymer

The effect of particle–matrix adhesion on the mechanical behavior of glass filled epoxies. Part 2. A study on fracture toughness

Takafumi Kawaguchi*, Raymond A. Pearson

Materials Science and Engineering, Lehigh University, 5 East Packer Avenue, Bethlehem, PA 18015, USA

Received 21 October 2002; received in revised form 18 April 2003; accepted 21 April 2003

Abstract

The static fracture toughness behavior of glass filled epoxies was studied using single-edge-notched 3 point bend (SEN-3PB) tests. Three different types of glass reinforcements, large glass spheres (LGS), small glass spheres (SGS), and glass fibers (GF), were examined. The surface of each type of filler was treated to either promote or inhibit particle–matrix adhesion. The volume fraction of filler studied ranged from 10 to 30 vol%. Special attention was given to the effect of particle surface treatment and/or moisture exposure on fracture toughness. Interestingly, moisture exposure resulted in improved toughness in the case of poor adhesion at the matrix–particle interface for LGS and GF filled epoxies. Transmission optical microscopy and scanning electron microscopy were used to examine the process zone in SEN-3PB specimens. These observations along with yield stress measurements suggest that the improved toughness was due to enhanced shear yielding of the matrix due to poor adhesion at the matrix–particle interface and increased matrix ductility due to the plasticizing effect of the absorbed moisture.
© 2003 Elsevier Science Ltd. All rights reserved.

Keywords: Epoxy; Fracture toughness; Composite

1. Introduction

The toughening of epoxies has been extensively studied and several successful approaches to toughening have been found. These methods include chemical modification of epoxy molecular structure [1], addition of a second rubbery phase [2,3], incorporation of inorganic fillers [4], hybrid toughening utilizing elastomeric and inorganic fillers [5,6], void toughening [7,8], and the use of thermoplastic particles [9,10]. In the case of rubber toughened epoxies, it has been shown that cavitation of rubber particles induces shear yielding of epoxy-matrix that results in effective energy dissipation at the crack tip and, hence, improved toughness. Unfortunately, the addition of rubber particles usually results in a decrease in yield stress that may limit the application of the material in some instances. In the case of filled epoxies, it has been suggested that there is a possibility that toughness can be improved without the loss of strength of the material [11]. Indeed, superior strength and stiffness may be why inorganic filled epoxies have been of great interest to many investigators.

For inorganic filled epoxies, it is known that the toughening mechanisms are quite different from those in rubber toughened epoxies. For inorganic spheres, toughening by microcracking [12] and crack pinning [13] have been proposed and are widely accepted as important toughening mechanisms. Microshear banding has also been proposed for epoxy composites reinforced with glass spheres [14,15]. For epoxies filled with inorganic fibers, toughening by microcracking [12], crack pinning [13], fiber bridging [16] followed by fiber breakage, crack deflection [17], and fiber dedonding [18] followed by fiber pull-out [19] have been proposed.

Because of the increasing usage of epoxy composites in severe environments such as high temperature and high humidity there is a need to improve our understanding of the performance of the epoxy composites under such conditions. Therefore, the resistance of epoxy composites to high heat and humidity has attracted much attention. For example, application of various silane coupling agents has been found to be an effective means to improve adhesion between inorganic reinforcements and epoxy-matrix and,

* Corresponding author. Present address: R & D Department, Osaka Gas Company Ltd, 6-19-9 Torishima, Konohana-ku, Osaka 554 0051, Japan. Tel.: +81-6-6463-3441; fax: +81-6-6462-3436.
E-mail address: tkawa@osakagas.co.jp

0032-3861/03/$ - see front matter © 2003 Elsevier Science Ltd. All rights reserved.
doi:10.1016/S0032-3861(03)00372-0

hence, increases the resistance of epoxy-matrix composites to hot, humid environments [20]. Although there are many reports that focus on the effect of coupling agents on the resistance of epoxy composites to heat and humidity [20–25], few provide insight on the role of particle–matrix adhesion and changes in the mechanical behavior of the matrix on the fracture toughness of the composite. Of course, moisture can affect both the properties of matrix as well as particle–matrix adhesion, thus resulting in a rather complicated subject.

In the present study, the effect of moisture and particle–matrix adhesion on the fracture toughness of glass filled epoxy composites was systematically investigated. Three different types of reinforcements, large glass spheres (LGS), small glass spheres (SGS), and glass fibers (GF), were used. Surface treatment and filler loadings were varied in a systematic fashion. Transmission optical microscopy (OM) and scanning electron microscopy (SEM) were used to inspect the process zone. Measurements of yield stress and cohesive strength found in a previous report [26] were extensively used to clarify the mechanism of toughening. Special attention was paid to the matrix shear yielding toughening mechanism. The results in this study will also be used to explain the toughening mechanism in fatigue crack propagation [27].

2. Experimental

2.1. Materials

A description of the materials used in this study is shown in Table 1. The epoxy system consisted of diglycidyl ether of bisphenol-A (DGEBA) based epoxy resin (Dow Chemical DER®331, epoxide equivalent weight = 182–192 g/equiv. wt) and bisphenol-A (resin modifier) cured with piperidine.

Three types of reinforcements were used in this study. Two types were glass spheres (Potters Industry Spheriglass®2900 glass spheres and Spheriglass®10000E). According to the supplier, these glass spheres have a mean diameter of 42 and 3.8 μm, respectively. The third type of reinforcement consisted of GF (Owens Corning milled fiber 739DD 1/16″) that have a mean diameter of 15.8 μm and a nominal bulk density of 0.50 g/cm^3.

2.2. Sample preparation

Three different surface treatments were studied for each type of reinforcement. Some of the reinforcements were treated with 1 wt% solutions (95 wt% methanol and 5 wt% water) of aminopropyltrimethoxysilane (APS) or *n*-butyltrimethoxysilane (*n*BS) and rinsed with methanol. The molecular structures of these adhesion promoters are shown in Fig. 1. As a control (third treatment), reinforcements with no adhesion promoters on the surfaces were simply washed with methanol. The details for the interaction of adhesion promoters with epoxy-matrix is described elsewhere [26].

The epoxy resin and 24 phr bisphenol-A (phr: part per hundred parts resin by weight) were mixed at 180 °C under vacuum and cooled to 80 °C. Then, 10, 20, or 30 vol% of reinforcement was added and mixed under vacuum. Next, 5 phr of piperidine was added and mixed for about 10 min under vacuum. The mixture was poured into a mold, that had been preheated at 160 °C. Curing was performed at 160 °C for 6 h. Specimens were cut from the plaques prepared by this procedure. The designation for each material prepared is shown in Table 2.

2.3. Moisture exposure

Specimens were kept in a humidity chamber set at 85 °C and 85 RH% for 1350 h in order to absorb an equilibrium moisture content of about 1.3 wt% [26].

Table 1
Materials used in this study and their properties

	Materials	Properties	Designation
Matrix resin	Diglycidyl ether of bisphenol-A (DGEBA) DER®331	Epoxide equivalent weight = 182–192	331
Resin modifier	Bisphenol A	Melting point = 153 °C	BisA
Curing agent	Piperidine	Boiling point = 106 °C	Pip
Reinforcement types			
LGS	Spheriglass®2900	Mean diameter = 42 μm	LGS
SGS	Spheriglass®10000E	Mean diameter = 3.8 μm	SGS
Glass fibers	739DD 1.6 mm	Mean diameter = 15.8 μm, Mean length = 399 μm, Nominal density = 0.50 g/cm^3	GF
Surface treatments	Agents	Designation	
Adhesion promoter	Aminopropyltrimethoxysilane	APS	
	n-Butyltrimethoxysilane	*n*BS	
No adhesion promoter	Washed by methanol	NT	

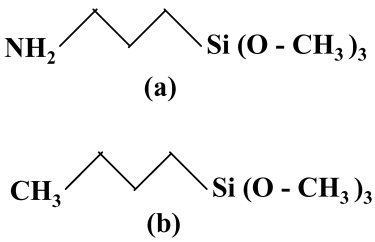

Fig. 1. The molecular structures of those adhesion promoters used in this study (a) aminopropyltrimethoxysilane and (b) *n*-butyltrimethoxysilane.

2.4. Single-edge-notched 3 point bending (SEN-3PB) fracture toughness tests

For the purpose of determining critical stress intensity factors (K_{IC}), single-edge-notched 3 point bending (SEN-3PB) tests were performed using a screw-driven Instron universal testing machine, type 5567, with a cross-head speed of 2.54 mm/min. The thickness (B) and width (W) of the specimens were 6.0 and 12.0 mm, respectively. Initial cracks were introduced by tapping razor blades chilled in liquid nitrogen at the base of a notch.

K_{IC} values were determined using the equations [14]

$$K_{IC} = \frac{3PSa^{1/2}}{2BW^2} f\left(\frac{a}{W}\right),$$

$$f\left(\frac{a}{W}\right) = 1.93 - 3.07\left(\frac{a}{W}\right) + 14.53\left(\frac{a}{W}\right)^2 - 25.11\left(\frac{a}{W}\right)^3 + 25.8\left(\frac{a}{W}\right)^4 \quad (1)$$

where P is the load at failure, S is the span length, a is the crack length. Reported K_{IC} values are the average of at least five tests.

2.5. Yield stress measurements

Yield stress was measured in compression according to the method described in ASTM D695 [28] using an Instron universal testing machine type 5567. Tetragonal-shaped specimens of 6 mm × 6 mm × 12 mm were used. The cross-head speed was 1.3 mm/min. Reported yield strengths are the average of at least three tests.

2.6. SEM observations

Fracture surfaces of SEN-3PB tests were observed using a JEOL 6300F or Philips XL30 SEM with an acceleration voltage of 5 kV. Fracture surfaces were covered with sputtered Au–Pd before examination.

2.7. OM observations

Fractured SEN-3PB specimens were mounted in a room temperature-cured epoxy and ground perpendicular to the fracture surface and along the width of the specimen using standard petrographic techniques. Specimens were ground to approximately half the thickness to guarantee that the observation of the deformation mechanisms in the plane strain region. Ground surfaces were polished and subsequently bonded to petrographic-grade slide glasses. The excess mount was removed using a diamond saw and the sample on the slide was ground to a thickness of about 100 mm. The ground surfaces were again polished. Samples

Table 2
Materials prepared in this study and their designations

Matrix	Reinforcements	Vol% of reinforcements	Surface treatments of reinforcements	Designation[a]
331-BisA-Pip	None	–	–	Neat
	LGS	10	APS	LGS(10)-APS
			*n*BS	LGS(10)-*n*BS
			NT	LGS(10)-NT
		20	APS	LGS(20)-APS
			*n*BS	LGS(20)-*n*BS
		30	APS	LGS(30)-APS
			*n*BS	LGS(30)-*n*BS
	SGS	10	APS	SGS(10)-APS
			*n*BS	SGS(10)-*n*BS
			NT	SGS(10)-NT
		20	APS	SGS(20)-APS
			*n*BS	SGS(20)-*n*BS
		30	APS	SGS(30)-APS
			*n*BS	SGS(30)-*n*BS
	GF	10	APS	GF(10)-APS
			*n*BS	GF(10)-*n*BS
			NT	GF(10)-NT
		20	APS	GF(20)-APS
			*n*BS	GF(20)-*n*BS

[a] B and A at the end of each designation shows *before* moisture treatment and *after* moisture treatment, respectively.

prepared by the method mentioned above [29] were observed with an Olympus BH2 transmission optical microscope (OM).

3. Results and discussion

In this section, the results of K_{IC} measurements, SEM observations of fracture surfaces in SEN-3PB tests, OM observations of sub-surface damage zone in SEN-3PB are presented. Note that the details of the yield stress and cohesive strength measurements are discussed in a previous report [26]. Briefly, the compressive yield strength increases with increasing filler content. Moreover, the yield strength increases more when short GF are used and systematically decreases after moisture exposure.

3.1. K_{IC} measurements

Figs. 2–4 contain the results of K_{IC} measurements for the specimens with different reinforcements before and after moisture exposure. For the specimens reinforced with LGS (Fig. 2), the *n*BS treatment resulted in higher fracture toughness before and after moisture exposure. In all cases, the fracture toughness was observed to increase with increasing volume fraction of LGS (before moisture exposure). The improvement in fracture toughness of epoxies filled with APS treated LGS was small compared to those with *n*BS treated LGS. Interestingly, after moisture exposure, the fracture toughness of epoxies filled with *n*BS treated LGS exhibited a maximum at 10 vol%.

For SGS reinforced epoxy, the results were significantly different. In all cases, the fracture toughness improved with the addition of SGS. However, now the greatest improvement in fracture toughness was observed for the APS treated SGS (before moisture absorption). Again, the *n*BS treated spheres resulted in filled epoxies with a maximum in fracture toughness at 10 vol%. However, the toughest material in this series was the epoxy filled with 30 vol% APS treated SGS.

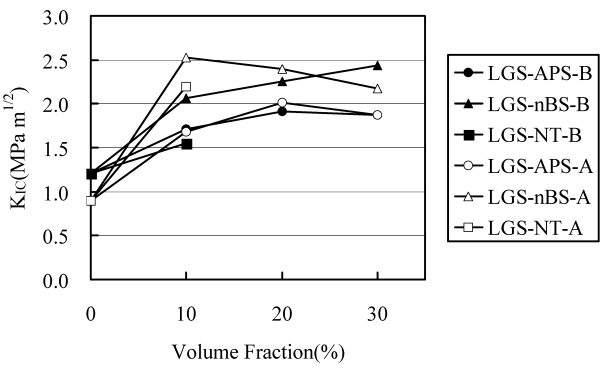

Fig. 2. In general, fracture toughness increases with filler content for LGS filled epoxies. After moisture exposure, the fracture toughness tends to exhibit a maximum at 10 vol%.

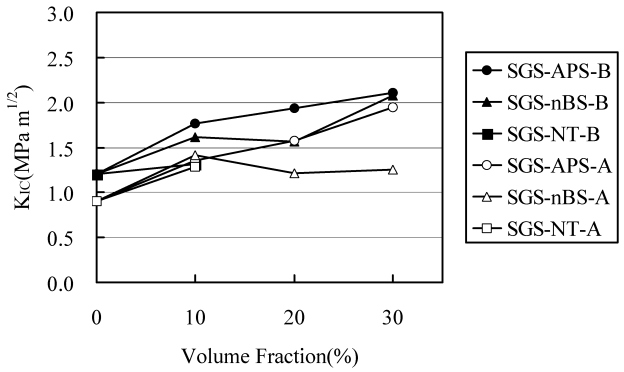

Fig. 3. In general, fracture toughness increases with filler content for SGS filled epoxies. After moisture exposure, the fracture toughness tends to exhibit a maximum when the particle–matrix adhesion is poor.

For the specimens reinforced with GF (Fig. 4), the increase in K_{IC} was also observed with the increase in volume fraction of GF before moisture exposure. The change in K_{IC} of the specimens with APS treated GF was small compared to those with *n*BS treated GF, which is the same trend as with LGS. Increase of K_{IC} was observed for the case of *n*BS treated GF.

3.2. Relationship between K_{IC} and yield stress

Irwin's model [30] can be used to relate the fracture toughness to the plastic zone size

$$r_p = \frac{1}{6\pi}\frac{K_{IC}^2}{\sigma_y^2} \tag{2}$$

where r_p is the plastic zone size and σ_y is yield stress. Eq. (2) suggests that a lower yield stress will result in a larger plastic zone and, in turn, can increase toughness.

Figs. 5 and 6 show the relationship between K_{IC} and yield stress for composites reinforced with different reinforcements. As seen in Fig. 5, epoxies filled with *n*BS treated LGS showed higher K_{IC} at higher yield stress before moisture exposure. Interestingly, the fracture toughness increases with yield strength (increasing LGS content). This result

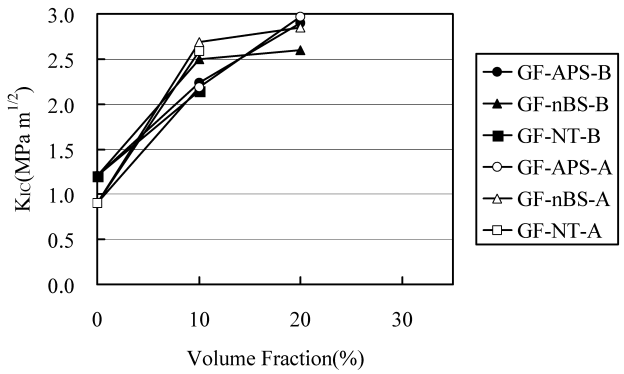

Fig. 4. Fracture toughness increases with filler content for GF filled epoxies.

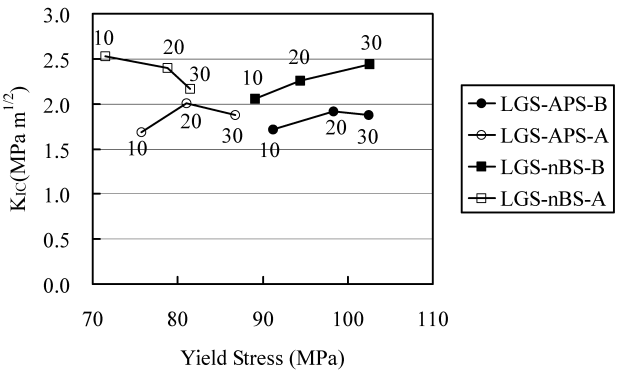

Fig. 5. For the LGS filled epoxies with poor adhesion, fracture toughness decreases with increasing yield strength. This result suggests that a shear yielding mechanism occurred.

suggests that the toughening mechanism before moisture exposure does not involve matrix plasticity. On the other hand, after moisture exposure, a drop in yield stress resulted in even higher fracture toughness. This decrease in fracture toughness with increasing filler after moisture exposure suggests a toughening mechanism involving matrix shear banding. For the case of epoxies containing APS treated LGS, the dependence of K_{IC} on yield stress showed little change before and after moisture exposure. This insensitivity to changes in matrix ductility suggests that the toughening mechanism does not involve matrix shear banding.

In the case of SGS, the dependence of K_{IC} on the yield stress showed the same trend as LGS. Again, epoxies filled with *n* BS treated spheres showed higher fracture toughness at a lower yield stress. The yield stress–toughness dependence, however, was smaller than that observed for LGS filled epoxies. For the case of epoxies filled with GF, higher yield stress (dry matrix) resulted in higher K_{IC}. However, the dependence of K_{IC} on yield stress was much smaller for *n* BS treated GF than for APS treated GF.

Although not shown in a figure, even the neat epoxy resin exhibited the same type of dependence as the APS treated specimens. The fact that neat specimens, which are essentially homogenous, did not obey the Irwin model

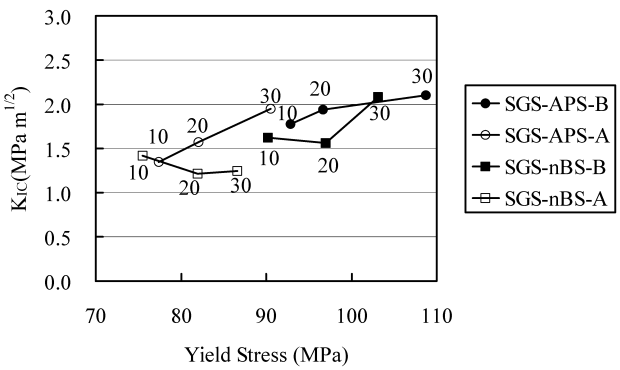

Fig. 6. For the SGS filled epoxies, fracture toughness increases with increasing yield strength. This result suggests that shear yielding is not involved in toughening.

suggests that the cohesive strength of the matrix decreased by plasticizing effect of water after moisture exposure. In fact, the results of cohesive strength measurement using the double notch 4 point bending tests showed that the cohesive strength of the matrix did indeed decrease after moisture exposure [26].

3.3. SEM observation of fracture surfaces of SEN-3PB test specimens

SEM was applied to elucidate the toughening in these particulate filled composites. Figs. 7 and 8 show the SEM images of the process zone on the fracture surface of SEN-3PB tests of LGS(10)-APS-B and LGS(10)-APS-A, respectively. The arrows above the figures indicate the direction of macroscopic crack propagation direction. In Fig. 7, features that can be attributed to crack pinning [5] are observed. There is also evidence that the matrix adhered well to glass spheres. In Fig. 8(a), features due to crack pinning can also be seen even after moisture exposure, and debonding between matrix and glass spheres was observed. Fig. 8(b) shows the image of a glass sphere that was about to debond from the matrix. Because of the triaxial tensile stress state at the crack tip, the matrix around the crack tip tries to expand in every direction. Strong adhesion between the matrix and glass spheres inhibited the expansion of the matrix resulting in the cohesive failure of the matrix.

Figs. 9 and 10 show the SEM images of the process zone on the fracture surface of SEN-3PB tests of LGS(10)-*n* BS-B and LGS(10)-*n* BS-A, respectively. In Fig. 9, debonding between epoxy-matrix and glass spheres is clearly observed. This result is consistent with the expectation based on the non-reactive head of this coupling agent [26]. On the other hand, in Fig. 10, significant matrix dilation around glass spheres can be clearly seen. The specimens, in this case, showed stable crack growth, and matrix dilation was observed over the entire fracture surface. The deformation of the matrix is similar to that of rubber toughened epoxy

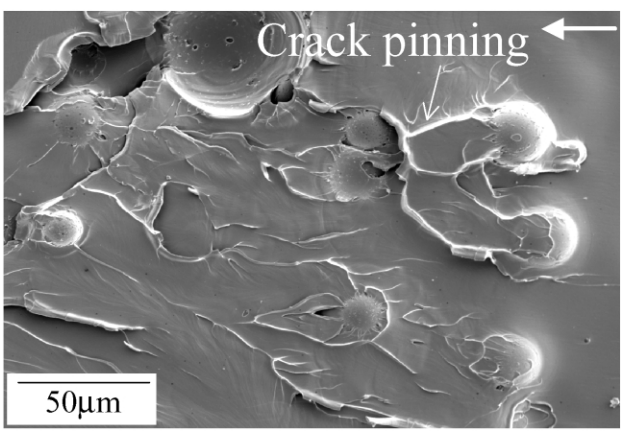

Fig. 7. An SEM image of the process zone on the fracture surface of SEN-3PB tests of LGS(10)-APS-B (i.e. before moisture treatment) that clearly shows crack pinning.

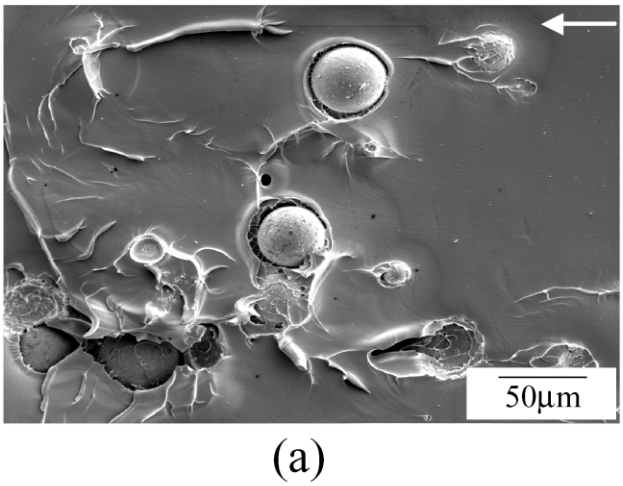

Fig. 8. SEM images of the process zone on the fracture surface of SEN-3PB tests of LGS(10)-APS-A (i.e. after moisture treatment) that clearly shows some particle–matrix debonding.

[5], which suggests that a shear matrix yielding mechanism was the dominant toughening mechanism in this case.

In the case of LGS(10)-NT-B and LGS(10)-NT-A, the debonding between matrix and glass spheres was also observed. The point where the fracture of the matrix occurred, however, was closer to the poles of the spheres compared to the equatorial sites in LGS(10)-*n*BS-B (Fig. 9). In the case of rigid spheres, it has been reported that the location of maximum stress depends on interfacial adhesion. When matrix–particle adhesion is strong, the maximum point of stress is at the poles of the spheres. The location of maximum stress shifts towards the equator as the matrix–particle adhesion becomes poorer [31]. After moisture treatment (LGS(10)-NT-A), the debonding at the epoxy-particle interface was more clearly observed than before moisture treatment. Although the dilatation of the matrix was also observed after moisture treatment, the degree of the matrix dilatation and the size of voids left by debonded particles were much smaller than those of LGS(10)-*n*BS-A.

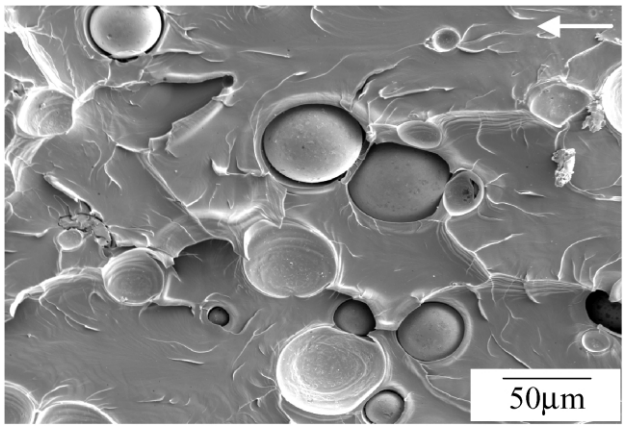

Fig. 9. An SEM image of the process zone on the fracture surface of SEN-3PB tests of LGS(10)-*n*BS-B that shows significant particle–matrix debonding.

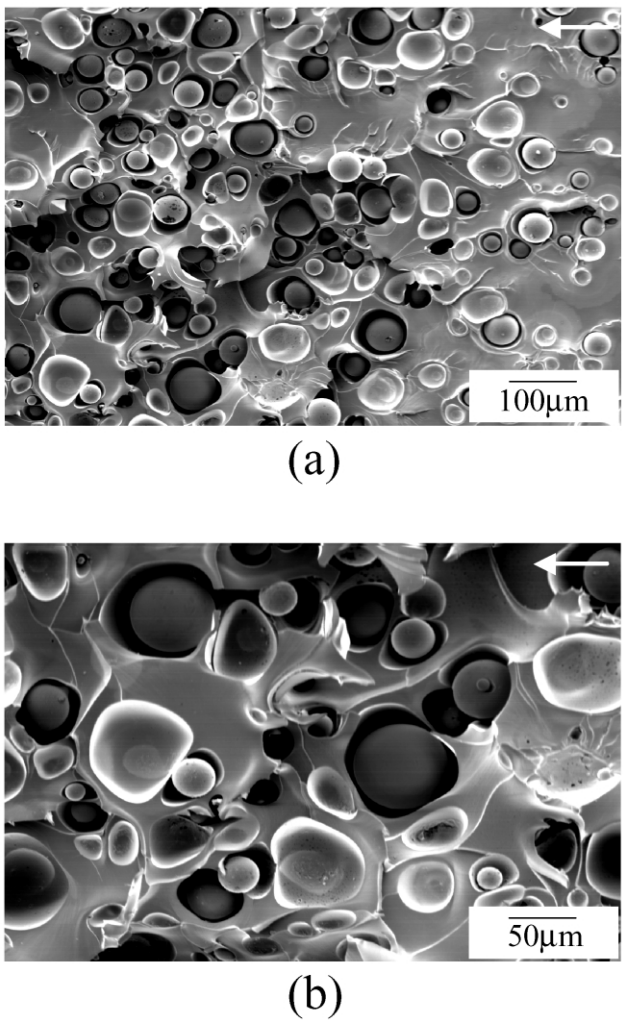

Fig. 10. SEM images of the process zone on the fracture surface of SEN-3PB tests of LGS(10)-*n*BS-A that shows significant particle–matrix debonding as well as increased matrix plasticity.

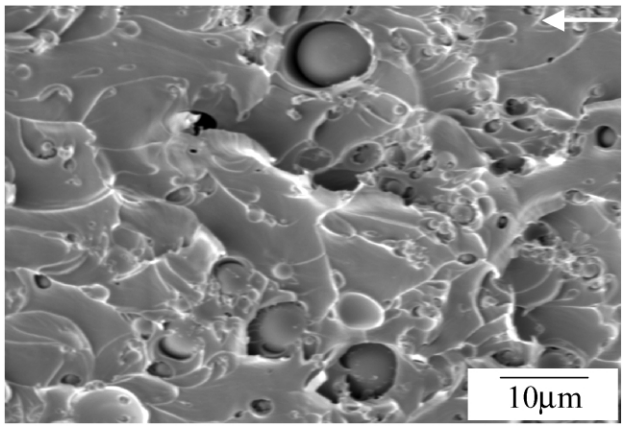

Fig. 11. An SEM image of the process zone on the fracture surface of SEN-3PB tests of SGS(10)-*n* BS-B that shows significant particle–matrix debonding.

Figs. 11 and 12 show the SEM images of the process zone on the fracture surface of SEN-3PB tests of SGS(10)-*n* BS-B and SGS(10)-*n* BS-A, respectively. Debonding can be seen clearly at the matrix–particle interface in Fig. 11 because of the poor matrix–particle adhesion. After moisture exposure, the plastic dilation of the matrix as well as debonding was observed (Fig. 12) which suggests that there was toughening due to matrix shear yielding. The shear yielding mechanism will be discussed in detail in Section 3.4. In the case of APS-treated SGS glass spheres were hardly seen because of the fact that the maximum stress was at the pole of the spheres due to strong matrix–particle adhesion and that the crack propagated at the pole of the spheres. Although a few spheres which were debonded from the matrix were observed after moisture treatment, the adhesion at the matrix–particle interface seemed to be still strong as fragments of the matrix appeared on the surface of the spheres.

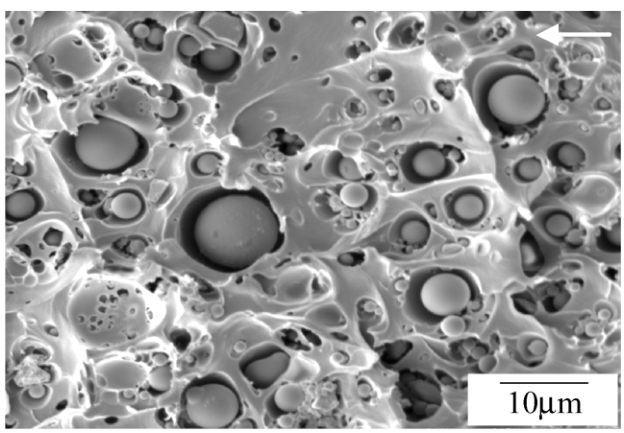

Fig. 12. An SEM images of the process zone on the fracture surface of SEN-3PB tests of SGS(10)-*n* BS-A that shows significant particle–matrix debonding with limited void growth.

3.4. TOM observations and discussion

Figs. 13 and 14 contain transmission optical micrographs of the process zone of LGS(10)-*n* BS-A and SGS(10)-*n* BS-A, respectively. Those images were taken under crossed polars. In Figs. 13 and 14, birefringence due to matrix shear yielding can be recognized. It can be concluded that poor matrix–particle adhesion allowed the matrix to debond easily upon loading resulting in the reduction of triaxial stress state and deformation of the matrix. The plasticizing effect of adsorbed moisture also contributed to the deformation of matrix. This conclusion is consistent with the mechanism proposed by Evans et al. [12]. This shear yielding mechanism can be considered to be similar to the one of the rubber toughening [2,3,32] and void toughening of epoxies [7,8] which are known to be effective ways of toughening epoxies. The sizes of the yield zone estimated from Figs. 13 and 14 were 89 and 12 μm for LGS(10)-*n* BS-A and SGS(10)-*n* BS-A, respectively. The yield zone size predicted from the Irwin's model were calculated to be 66 and 19 μm for LGS(10)-*n* BS-A and SGS(10)-*n* BS-A, respectively. The fact that shear yielding was observed for those systems by optical microscope was in good agreement with the expectations based on Irwin's model as mentioned above. In other words, measurements of yield stress and fracture toughness of composites with different volume fraction of reinforcements can used for understanding toughening mechanisms only when a shear yielding mechanism is present.

In the case of rubber toughened epoxies, it has been reported that the size of the rubber phase that gives effective toughening due to shear yielding is less than 10 μm [32]. The result of this present study showed that the relatively large 40 μm spheres were more effective in forming shear yield bands than small 3 μm spheres. There are two possible reasons for these observations. The first one is based on the dependence of debonding stress on the sphere size. Gent proposed that the stress necessary to cause the debonding

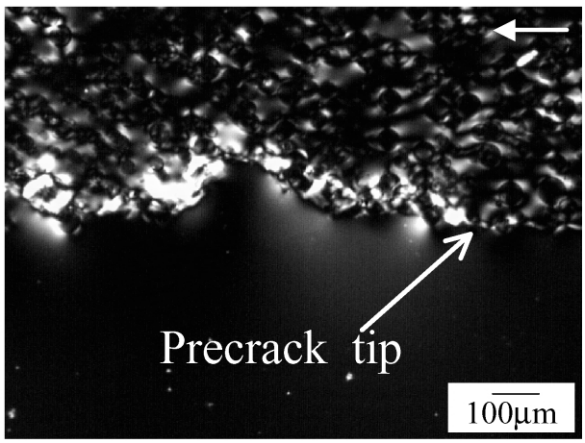

Fig. 13. A cross-sectional OM image of LGS(10)-*n* BS-A revealing the significant depth and length of the plastic zone.

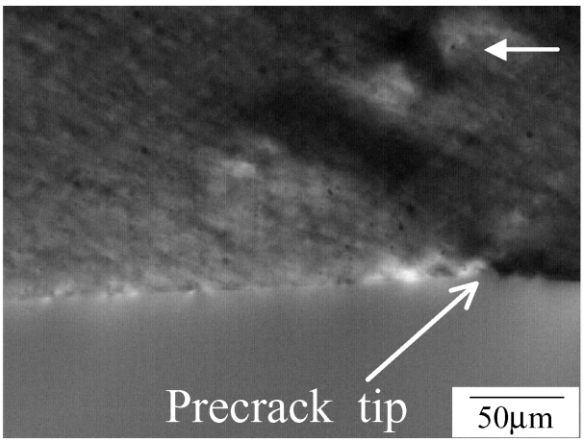

Fig. 14. A cross-sectional OM images of SGS(10)-*n*BS-A revealing the lack of significant plastic zone development.

(σ_a) is expressed by Eq. (3) [33]

$$\sigma_a^2 = \frac{8\pi G_a E}{3kr\sin 2\theta} \tag{3}$$

where G_a is the bond fracture energy per unit of bonded surface, E is Young's modulus of the composite, k is a constant, r is the radius of the sphere, and θ is the polar angle. This equation shows that σ_a increases with the decrease in sphere size which results in a lower probability for the debonding of small spheres and, hence, a lower probability for shear yielding of matrix. The other possible explanation for our results is based on the discussion on the inter-particle distance. The inter-particle distance (ID) of spheres in a composite can be calculated using the equation [34]

$$\mathrm{ID} = D_P\left\{\left(\frac{\pi}{6V_f}\right)^{1/3} - 1\right\} \tag{4}$$

where D_p is the particle diameter, and V_f is the volume fraction of the particle. As the equation shows, the ID decreases with the decrease in particle diameter. In the case of LGS, ID was estimated to be from 9 μm (30 vol%) to 31 μm (10 vol%) from Eq. (4). On the other hand, in SGS, ID was calculated to be 0.6 μm (30 vol%) to 2.2 μm (10 vol%). Because of the small ID in SGS reinforced composites and the rigidity of glass spheres, the shear band growth can be limited within a small area resulting in relatively lower toughness.

4. Conclusions

The static fracture toughness behavior of several glass filled epoxies was studied using SEN-3PB tests. Three different types of glass reinforcements, LGS, SGS, and GF, were used with different surface treatments and the effect of different surface treatments and moisture exposure on fracture toughness was carefully investigated. Under as molded conditions, fracture toughness was found to increase with increasing filler content and was not affected by changes in particle–matrix adhesion. After moisture exposure, improved toughness was observed in LGS and GF filled systems when the adhesion at the matrix–particle interface was poor. The results of observation by OM and SEM of the process zone, as well as the measurement results of yield stress suggested that there was a drastic change in the toughening mechanism in the specimens with poor matrix–particle adhesion after moisture exposure. Those studies revealed that the improved toughness was due to the shear yielding of the matrix enhanced by poor adhesion of the matrix–particle interface and the increased matrix ductility because of the adsorbed moisture. It was also found that the degree of shear yielding was strongly dependent on the size of the glass spheres after moisture exposure. The particle-size dependence of the fracture toughness of filled epoxies was explained by the magnitude of the debonding stress at the matrix–particle interface and the inter-particle distance.

Acknowledgements

This work was supported by Osaka Gas Co. Ltd in Japan.

References

[1] Sue H-J, Puckett PM, Bertram JL, Walker LL. In: Pearson RA, Sue H-J, Yee AF, editors. Toughening of plastics. ACS Symposium Series 759, Washington, DC: American Chemical Society; 2000. p. 171.
[2] Kinloch AJ, Shaw SJ, Tod DA, Hunston DL. Polymer 1983;24:1341.
[3] Pearson RA, Yee AF. J Mater Sci 1986;21:2475.
[4] Kawaguchi T, Pearson RA. Polymer 2003; in press.
[5] Azimi HR, Pearson RA, Hertzberg RW. J Appl Polym Sci 1995;58:449.
[6] Kinloch AJ, Maxwell D, Young RJ. J Mater Sci Lett 1985;4:1276.
[7] Bagheri B, Pearson RA. Polymer 1996;37:4529.
[8] Lesser AJ, Kody RS, Crawford ED. In: Pearson RA, Sue H-J, Yee AF, editors. Toughening of plastics. ACS Symposium Series 759, Washington, DC: American Chemical Society; 2000. p. 159.
[9] Bucknall CB, Gilbert AH. Polymer 1989;30:213.
[10] Pearson RA, Yee AF. Polymer 1993;34:3658.
[11] Nielsen LE. J Appl Polym Sci 1966;10:97.
[12] Evans AG, Williams S, Beaumont PWR. J Mater Sci 1985;20:3668.
[13] Lange FF. Philos Mag 1971;22:983.
[14] Lee J, Yee AF. Polymer 2000;41:8375.
[15] Lee J, Yee AF. Polymer 2001;42:577.
[16] Evans AG, McMeeking RM. Acta Metall 1986;34:2435.
[17] Faber KT, Evans AG. Acta Metall 1983;31:565.
[18] Wells JK, Beaumont PWR. J Mater Sci 1988;23:1274.
[19] Thouless MD, Sbaizero O, Sigl LS, Evans AG. J Am Ceram Soc 1989;72:525.
[20] Pape PG, Plueddemann EP. J Adhes Sci Technol 1991;5:831.
[21] Ishai O. Polym Engng Sci 1975;15:486.
[22] Ishai O. Polym Engng Sci 1975;15:491.
[23] Morii T, Tanimoto T, Maekawa Z, Hamada H, Kiyoshumi K, Ichibashi H. Polym Composites 1993;1:113.
[24] Phillips MG. Composites 1983;14:270.
[25] Wang TWH, Blum FD. Polym Prepr 1995;36:817.

[26] Kawaguchi T, Pearson RA. Polymer 2003; in press.
[27] Kawaguchi T, Pearson RA, submitted to Polymer.
[28] Annual Book of ASTM Standards. 2001; 08.01: pp. 76.
[29] Sue H-J, Pearson RA, Parker DS, Huang J, Yee AF. Polym Prepr 1988;29:147.
[30] Irwin GR. J Appl Mech 1957;24:361.
[31] Dekkers ME, Heikens D. J Mater Sci 1984;19:3271.
[32] Pearson RA, Yee AF. J Mater Sci 1991;26:3828.
[33] Gent AN. J Mater Sci 1980;15:2884.
[34] DiBerardino MF, Pearson RA. In: Pearson RA, Sue H-J, Yee AF, editors. Toughening of plastics. ACS Symposium Series 759, Washington, DC: American Chemical Society; 2000. p. 213.